Supplementary Information

Comparison between simulated powder X-ray diffraction spectra of different CDW phases

Figure S1 shows semi-log plots of the simulated powder X-ray diffraction (pXRD) patterns for the seven charge density wave (CDW) phases obtained from our calculations. We focus on pXRD patterns because, in real samples, domains with different orientations of CDW patterns are likely to coexist, resulting in averaged XRD signals. All CDW phases exhibit clear superstructure peaks compared to the primitive $P\bar{3}m1$ phase (not shown). Notably, the A, B, C, and D phases display highly similar pXRD patterns, despite having different space group symmetries (see Table I in the main text).

Figure S2(a) illustrates this similarity more clearly. Here, the difference between each phase is defined as the integral of the absolute value of the pXRD signal over the entire angle range. The results reveal three distinct groups with similar pXRD spectra: (A, B, C, D), (E, G), and (F). In particular, the A and D phases show nearly indistinguishable pXRD patterns (see Fig. S2(a)), even though their CDW patterns and unfolded band structures differ significantly (compare Fig.1(a) and 1(d) in the main text, and see Fig.S2(b)). It is striking that two CDW phases with distinct superstructure periodicities—$2 \times 2 \times 1$ for A and $2 \times 2 \times 2$ for D—and different electronic structures yield nearly identical pXRD patterns. The origin of this behavior remains under investigation.

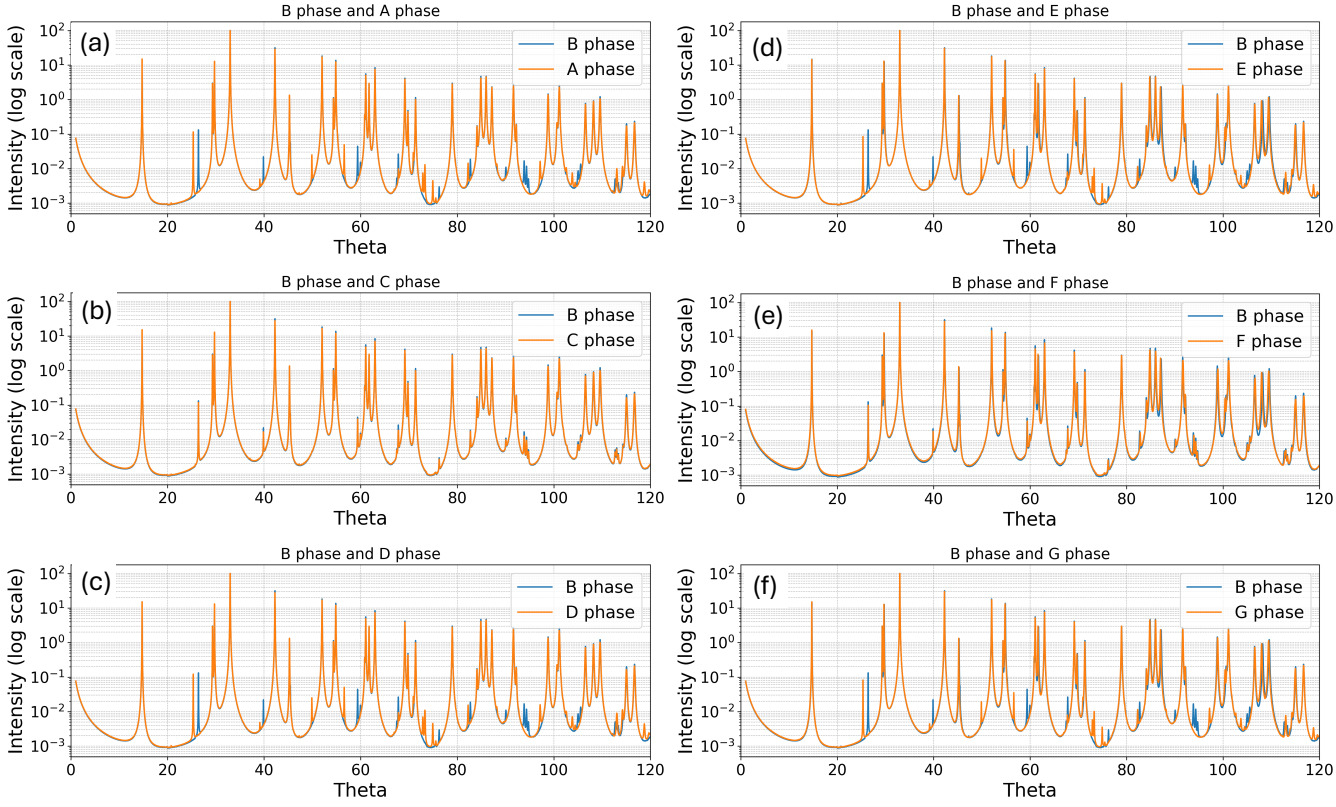

FIG. S1: Semi-log plots of simulated powder X-ray diffraction (pXRD) patterns of seven CDW phases obtained from our calculations. Each panel compares the three-fold symmetric B-phase ($P\bar{3}c1$) with other monoclinic (A, C, $\cdots$ G) phases.

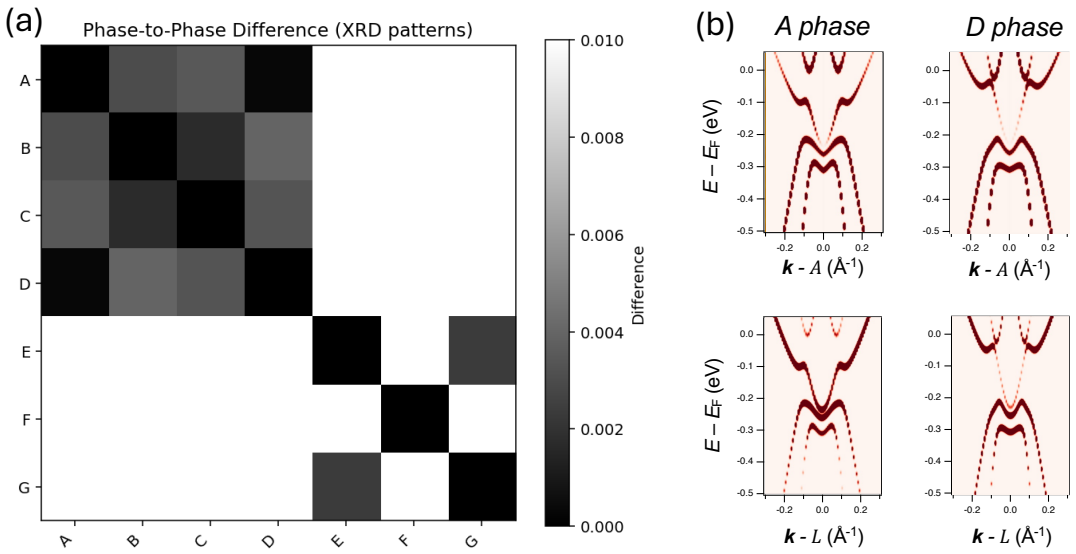

FIG. S2: (a) Difference matrix heatmap of the seven CDW phases (in arbitrary unit), where darker (brighter) color indicate more similar (different) powder X-ray diffraction patterns between two structures. (b) Unfolded band spectra of the A and D CDW phases, in the vicinity of A and L points.

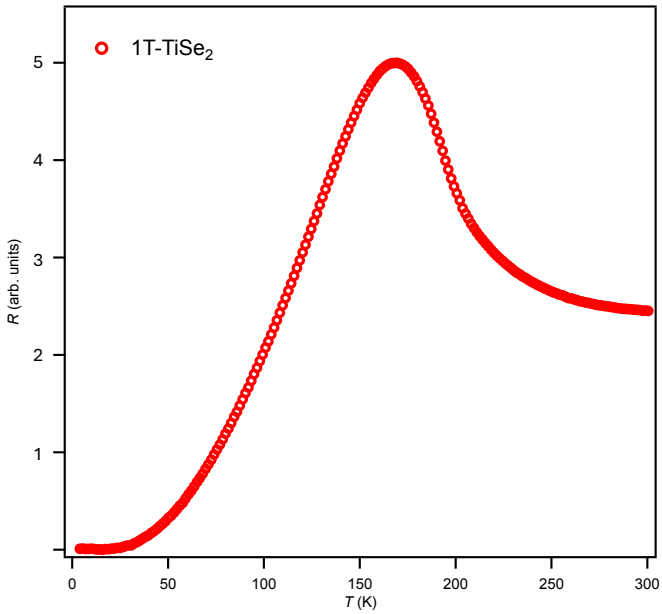

FIG. S3: Temperature-dependent resistivity curve of single-crystalline 1T-$TiSe_2$. The measurement was performed over the temperature range of 4–300 K.

Temperature-dependent resistivity data

Figure S3 plots the temperature-dependent resistivity data measured from our sample, which shows the resistivity peak around T = 169 K, consistently with previous observations (H. Ueda *et al.*, *Phys. Rev. Res.* **3**, L022003 (2021), etc.).

Comparison between ARPES and band-unfolding spectra

Here we compare our ARPES spectra at T = 180 (see Fig. S4(a)) and 20 K (Fig. S4(b)) with band-unfolding spectra of 7 phases (denoted as A, B, C, D, E, F, G phases) from DFT calculations. At 180 K (Fig. S4(a)) an inverted parabolic-like valence bands, with very weak conduction-band-like signatures, are observed from the ARPES data. From the comparison, the B and C phases share similar character, while the A and D phases show M-shaped valence bands around -0.2 eV, unlike the experimental observation. At L point, a flat-band-like signature is observed above -0.2 eV, below which signal is almost absent. The C phase shows similar band shape, while the B phase hosts visible parabolic-like dispersion between -0.3 and -0.1 eV. Based on these observations, the C phase can be considered the best match to the ARPES data at 180 K. At 20 K (Fig. S4(b)), below the second CDW transition temperature, the ARPES data reveal a double-dot-like feature near the Fermi level at the A point, and at the L point a V-shaped conduction band touching valence bands are seen. The inverted parabolic-like valence bands at the A-point match with B and C phases, while the presence of V-shaped conduction-like band above -0.2 eV and the absence of gap between the valence and conduction bands is consistent with the A and B phases. From these, we deduce that the B phase well-matches with the APRES spectra at 20 K, with possibly small fraction of A phase. Note that the mismatch between the ARPES and band-unfolded DFT spectra can be attributed to the absence of matrix element effects in the DFT results, and also to the potential inhomogeneity arising from the mixure of different CDW phases in the sample.

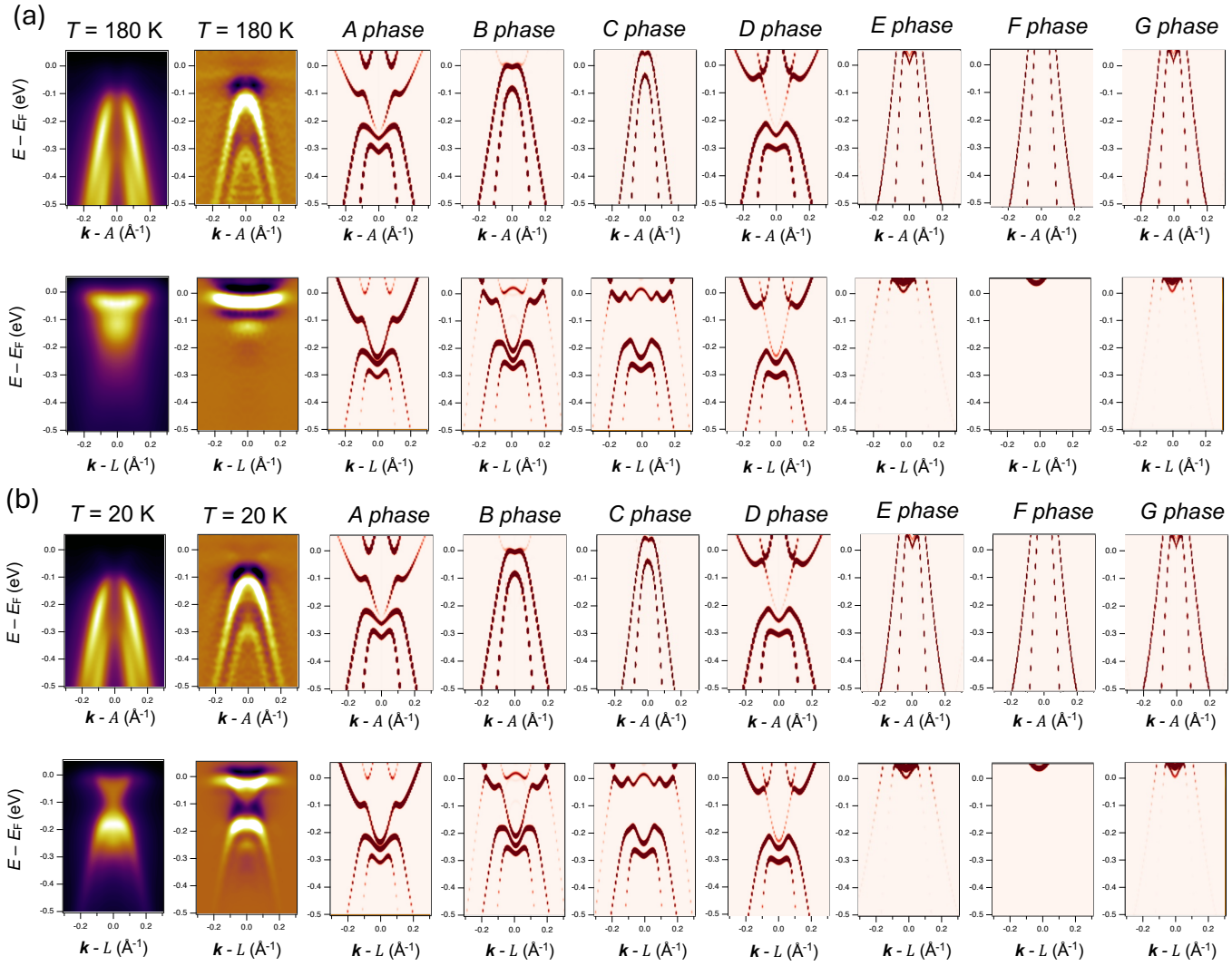

FIG. S4: (a, b) ARPES and DFT band structures. Left: Raw and second-derivative ARPES data at the A and L points for 180 K and 20 K, taken using 75 eV photon. Right: DFT band structures for each phase. At 180 K, the ARPES data show a parabolic band at the A point (consistent with the B and C phases) and a flat band at the L point (matching the C phase). At 20 K, below the second phase transition, the ARPES data exhibit a double-dot-like feature at A and a V-shaped band at L, both aligning with the A phase in DFT calculations.